3-D Strain Fields Using Embedded DSPI: Pilot Study

Gaetano Restivo[a], Gary L. Cloud[b], Rob M. Beaudry[b], Basavaraju B. Raju[c]
[b]*Dipartimento di Meccanica, Università degli Studi di Palermo, viale delle Scienze - 90128 Palermo, ITALY, email: restivo@dima.unipa.it*
[a] *Department of Mechanical Engineering, Michigan State University, East Lansing, MI – 48824,USA e-mail: cloud@egr.msu.edu, beaudry2@msu.edu*
[c] *U.S. Army Tank Automotive Command, Warren, MI – 48397, USA, email: rajub@tacom.army.mil*

ABSTRACT
Interior strain fields in polymethylmethacrylate thick specimens are measured by an embedded digital speckle pattern interferometry (DSPI) method. The specimens contain an embedded reflecting-scattering surface in an interior plane. This is obtained by bonding two parts of the specimen with cyanoacrylate mixed with atomized aluminum powder. Specimens are beam-shaped and loaded in both four-point and three-point bending. The interferometer is in-plane sensitive and the phase difference maps are calculated using a four-step phase-shifting algorithm. The displacement maps are unwrapped and then, using least-square polynomial fitting, interpolated and differentiated to obtain strain. DSPI data is acquired for surface strain and strain within the material through the thickness. Comparisons using electrical resistance strain gages (RSGs) mounted on the specimens are performed for validation. Results obtained with "embedded" DSPI agree with RSGs, with errors averaging around 10%. Possible sources of errors have been analyzed. The method appears to be competitive with other techniques available in literature.

INTRODUCTION
Three-dimensional stress (or strain) fields are of great interest; this has led to the development of various theoretical, computational, and experimental techniques that are capable of observing internal information. These techniques lead to a better understanding in designing with advanced materials and in optimization of material- and energy- efficiencies.

The oldest and still most dependable technique for three-dimensional stress analysis is photoelasticity. 3-D Photoelasticity includes frozen stress, embedded polariscope and scattered light photoelasticity. In frozen stress photoelasticity [1], the desired photoelastic specimen is slowly heated in an oven while subjected to loading. Once the desired temperature is reached, the specimen remains loaded and is cooled slowly to room temperature. After cooling, loading is ceased and what remains is a specimen in a permanently stressed state, hence "frozen-stress". The stress throughout this specimen should then vary according to the applied loading conditions. The specimen is sliced into many pieces, normally quite thin, and each slice observed in the polariscope. Cutting the specimen does not adversely affect the stress state as long as proper procedures are used. Observing and analyzing subsequent slices is done to obtain the three-dimensional stress field through the thickness of the specimen. For the embedded polariscope [2], the polarizers and $\lambda/4$ plates are embedded at two parallel planes within the birefringent specimen. The specimen is then observed in the interferometer using the proper light source. Since the polariscope is within the specimen, any material not between these two planes will not contribute to stress fringes pattern after loading. Therefore, only the internal stress in the desired area is determined. Yet another three-dimensional photoelastic technique involves what is called optical slicing or scattered light photoelasticity [3]. The idea is to delimit a "slice" of the specimen between two plane laser beams. This involves the polarization properties of scattered light and the interference possibilities of the diffused beams to observe fringes.

An alternative to photoelasticity is the embedded-grid moiré method, which has been used several times [4-7]. More notable yet, the *multiple*-embedded-grid moiré method has been used to investigate multiple interior planes in a single specimen [8-9]. Strain was studied on the surface-, quarter-, and mid- planes of a thick polycarbonate specimen using both embedded moiré and embedded strain gages. Also, valuable insight and a correction procedure involving the errors caused by stress-induced gradients of refractive index when taking displacement and strain measurements on the interior of a solid were presented. Results obtained, after correction, agree with measurements made with embedded strain gages.

In the present work, a new approach to three-dimensional strain field investigation is proposed. Digital speckle pattern interferometry (DSPI) is used to observe an in-plane strain field on the interior plane of a polymethylmethacrylate specimen through two different thicknesses of material. DSPI [10] is a whole-field non-contact optical technique, thus far used for

Report Documentation Page

Form Approved
OMB No. 0704-0188

Public reporting burden for the collection of information is estimated to average 1 hour per response, including the time for reviewing instructions, searching existing data sources, gathering and maintaining the data needed, and completing and reviewing the collection of information. Send comments regarding this burden estimate or any other aspect of this collection of information, including suggestions for reducing this burden, to Washington Headquarters Services, Directorate for Information Operations and Reports, 1215 Jefferson Davis Highway, Suite 1204, Arlington VA 22202-4302. Respondents should be aware that notwithstanding any other provision of law, no person shall be subject to a penalty for failing to comply with a collection of information if it does not display a currently valid OMB control number.

1. REPORT DATE	2. REPORT TYPE	3. DATES COVERED
07 JUN 2004	**Journal Article**	**03-02-2004 to 19-05-2004**

4. TITLE AND SUBTITLE
3-D Strain Fields Using Embedded DSPI: Pilot Study

5a. CONTRACT NUMBER
5b. GRANT NUMBER
5c. PROGRAM ELEMENT NUMBER

6. AUTHOR(S)
Gaetano Restivo; Gary Cloud; Rob Beaudry; Basavaraju Raju

5d. PROJECT NUMBER
5e. TASK NUMBER
5f. WORK UNIT NUMBER

7. PERFORMING ORGANIZATION NAME(S) AND ADDRESS(ES)
Department of Mechanical Engineering,Michigan State University Engineering Building,428 S. Shaw Lane. Room 2555,East Lansing,Mi,48824

8. PERFORMING ORGANIZATION REPORT NUMBER
; #14179

9. SPONSORING/MONITORING AGENCY NAME(S) AND ADDRESS(ES)
U.S. Army TARDEC, 6501 East Eleven Mile Rd, Warren, Mi, 48397-5000

10. SPONSOR/MONITOR'S ACRONYM(S)
TARDEC

11. SPONSOR/MONITOR'S REPORT NUMBER(S)
#14179

12. DISTRIBUTION/AVAILABILITY STATEMENT
Approved for public release; distribution unlimited

13. SUPPLEMENTARY NOTES

14. ABSTRACT

Interior strain fields in polymethylmethacrylate thick specimens are measured by an embedded digital speckle pattern interferometry (DSPI) method. The specimens contain an embedded reflecting-scattering surface in an interior plane. This is obtained by bonding two parts of the specimen with cyanoacrylate mixed with atomized aluminum powder. Specimens are beam-shaped and loaded in both four-point and three-point bending. The interferometer is in-plane sensitive and the phase difference maps are calculated using a four-step phase-shifting algorithm. The displacement maps are unwrapped and then, using least-square polynomial fitting, interpolated and differentiated to obtain strain. DSPI data is acquired for surface strain and strain within the material through the thickness. Comparisons using electrical resistance strain gages (RSGs) mounted on the specimens are performed for validation. Results obtained with ?embedded? DSPI agree with RSGs, with errors averaging around 10%. Possible sources of errors have been analyzed. The method appears to be competitive with other techniques available in literature.

15. SUBJECT TERMS

16. SECURITY CLASSIFICATION OF:			17. LIMITATION OF ABSTRACT	18. NUMBER OF PAGES	19a. NAME OF RESPONSIBLE PERSON
a. REPORT	b. ABSTRACT	c. THIS PAGE			
unclassified	**unclassified**	**unclassified**	**Public Release**	**7**	

measuring the displacement components of an object's surface [11]; it is quick and easy to employ, has high sensitivity and resolution, and is appropriate for investigation of the strain field in cases having high spatial gradients. Here, a reflecting-scattering surface is embedded at an interior plane of an otherwise clear specimen to create the speckle effect. An in-plane sensitive phase-shifting speckle pattern interferometer is used. The speckle maps are recorded in the undeformed state and then again in the deformed state. These data are then digitized and manipulated by the computer using a "four-step" phase-shifting algorithm and image processing techniques [8]. Phase difference maps, which represent the whole-field displacement component, are least-squares fitted for strain calculation. Strain readings from electrical resistance strain gages (RSGs) are also recorded. These two data sets are then compared and presented in numerical and graphical form.

DSPI THEORY

In-plane sensitive DSPI setups, as shown in *Figure 1*, generally consist of a dual-beam illumination speckle pattern interferometer [10]. The in-plane displacement at the image plane, according to the sensitivity vector theory, is related to the phase difference through the following equation:

$$u(x,y) = \frac{\Delta\phi(x,y)}{2\pi} \cdot \frac{1}{2\sin\theta} \cdot \lambda, \tag{1}$$

where $\Delta\phi(x,y)$ is the optical phase change caused by object deformation, λ is the wavelength of light used, and θ is the illumination angle with respect to the viewing direction.

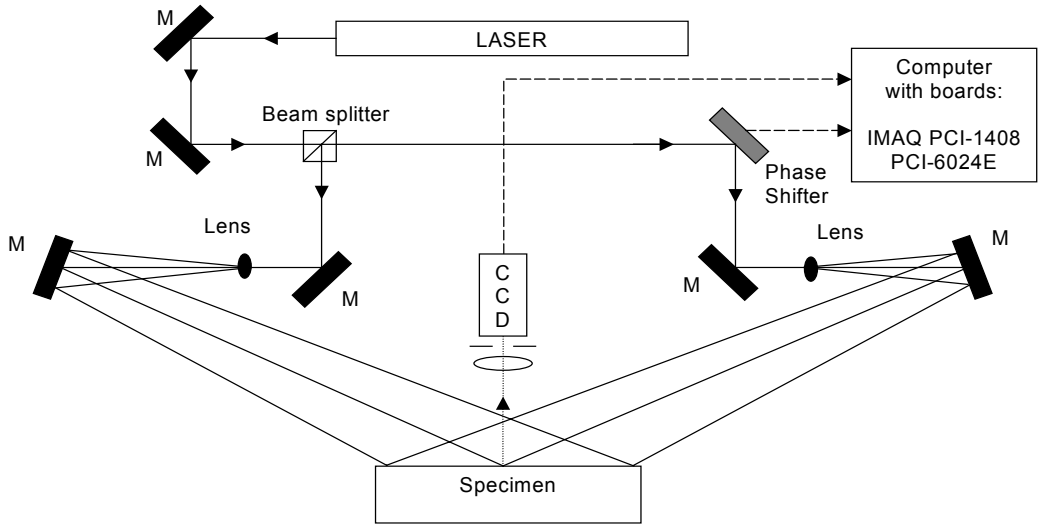

Figure 1. In-plane sensitive speckle pattern interferometer.

Phase-shifting, or phase-stepping, can be used to measure the phase data quantitatively. This technique involves one of the two coherent object beams being intentionally "phase-shifted", meaning its phase is shifted relative to the other beam. Then using multiple phase-shifts, the intensities of the speckle interference patterns are used to calculate the phase of one wavefront relative to the other. The "four-step" phase-shifting technique involves four sets, or steps, of equivalently phase-shifted interference intensity data that is sequentially captured before and after object deformation.

The intensity distribution, I_m, of the speckle interference pattern obtained is

$$I_m = I_A + I_B + 2\sqrt{I_A I_B}\cos\left(\phi + \psi_m\right) \tag{2}$$

where I_A and I_B are the intensities of the two object beams, ϕ is the phase-difference between the two beams, and ψ_m is the introduced phase-shift.

Consider the intensities I_1, I_2, I_3 and I_4, which correspond to the phase-shifts 0, $\pi/2$, π and $3\pi/2$ respectively. The interference wavefront phase distribution $\phi(x,y)$ at each image pixel is

$$\phi(x,y) = \arctan\left(\frac{I_4(x,y) - I_2(x,y)}{I_1(x,y) - I_3(x,y)}\right). \tag{3}$$

To determine the displacement of the object, the phase maps before deformation and after deformation must be subtracted. Therefore, the phase change due to object deformation, $\Delta\phi(x,y)$, is

$$\begin{aligned}\Delta\phi(x,y) &= \phi_{after}(x,y) - \phi_{before}(x,y) \\ &= \left[\phi(x,y) + \Delta\phi(x,y)\right] - \left[\phi(x,y)\right].\end{aligned} \tag{4}$$

This data yields the "phase-difference map" displaying "phase fringes" whose edges occur at every *n2π* phase change. The phase-difference map is then converted into the displacement field, according to the sensitivity vector relation in equation (1). In this setup, $\lambda = 0.633\mu m$ and $\theta = 30^{\circ}$, yielding the following equation describing the *x*-displacement field $u_x(x,y)$,

$$u_x(x,y) = 0.633\frac{\Delta\phi(x,y)}{2\pi}\left[\mu m\right] \tag{5}$$

Software written by one of the authors controls the phase-shifting piezo-electric transducer (PZT) and the frame grabber. After the four phase-shifted images have been captured, a two-dimensional look-up table (2-D LUT) [12] is used to calculate equation (3). Invalid low modulation pixels are then rejected using a threshold radius in the 2-D LUT. The "before" and "after" phase maps are then used to calculate the phase-difference map using equation (4); this map retains the invalid pixels from the previous maps. Filtering and local phase unwrapping [11] is then used to efficiently reduce noise and smooth the wrapped phase-difference map without blurring the 2π phase edges; fringe edges are identified as the sudden transition from white to black, and an example is shown in Figure 2. All the image processing steps are performed in real-time by the same software that controls the hardware.

(a) 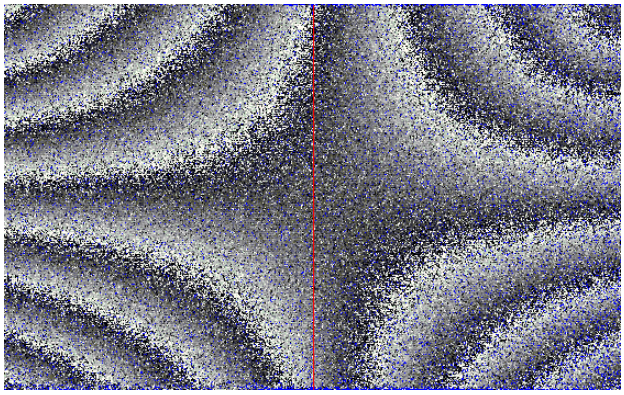 (b) 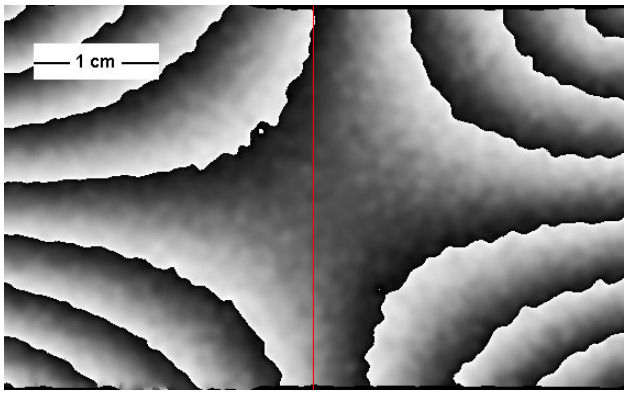

Figure 2. Smoothing and noise reduction without blurring around a 2π phase fringe-edge using filtering and local unwrapping.

Figure 2 shows the high sensitivity of DSPI: each fringe (phase difference of 2π), according to equation 5, corresponds to a displacement of $0.633\mu m$.

SPECIMENS FABRICATION

Two similar types of specimens, both beams, made of Polymethylmethacrylate (acrylic/plexi-glass/PMMA) were used. The first, designed for the main experimental results, consisted of two PMMA beams bonded together. The two pieces were such that one was of greater thickness than the other. They were bonded together using cyanoacrylate cement with the addition of atomized aluminum powder. The bond plane now acts as a reflecting-scattering surface much the same as if it were the surface of an opaque material (*Figure 3*). This specimen will be referred to as the "embedded" specimen, in the following

The second specimen, used for DSPI verification and data comparison, is a PMMA beam the size of the first but coated with a white-matte spray paint, also incorporating RSGs. This specimen will be referred to as "surface" specimen. It was used for comparison and validation purposes and to provide temperature compensation for the RSGs mounted on the embedded specimen. When the surface specimen was tested, temperature compensation was provided by the embedded specimen.

RSGs were then attached to the top and bottom of the specimen, perpendicular and co-linear to the scattering plane. *Figure 4* gives details about the embedded specimen and RSG placements.

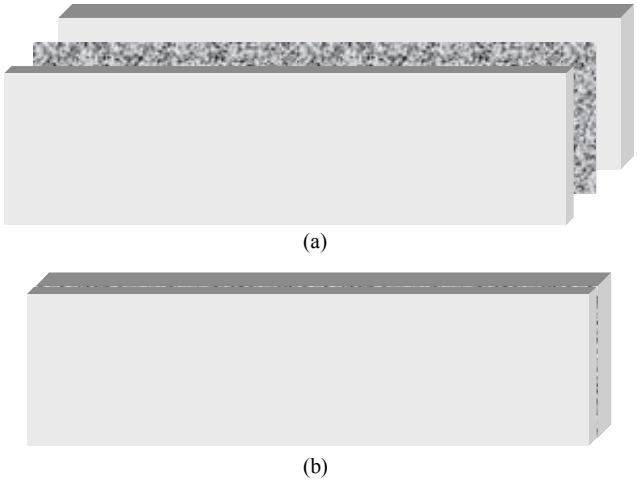

Figure 3. (a) Layers of the embedded specimen. (b) Assembled final product.

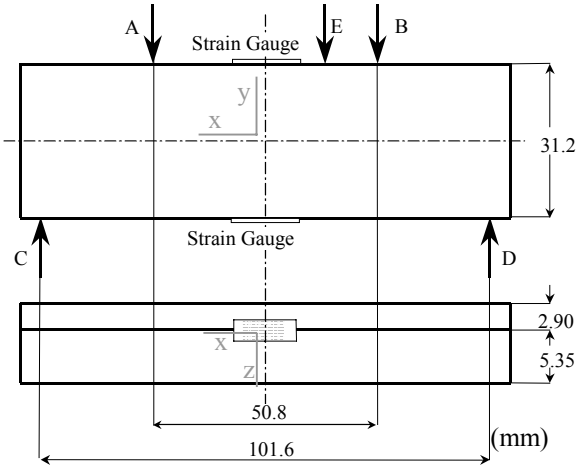

Figure 4. Embedded specimen dimensions and loading conditions. (A,B,C,D correspond to 4-point bending and E,C,D to 3-point.)

The RSGs installed, positioned for *x*-sensitivity, were type EA-13-240LZ-120 from Measurements Group. Application of any form of solvent was omitted as severe cracking damage occurred in early specimens. Degreaser caused similar effects on occasion and was therefore used sparingly.

EXPERIMENTAL PROCEDURE

After devising the necessary loading apparatus shown in *Figure 6*, one that could place the specimen in a position involving either four-point or three-point bending, the speckle pattern interferometer was set up to observe displacement in the *x*-direction. *Figure 1* represents the general schematic setup of the DSPI system in this experiment, *Figure 5* is a picture of the actual setup. The system includes a He-Ne laser ($\lambda = 0.633 \mu m$) running at ~10 mW, and 40X magnification diverging lenses. The mirror-mounted piezo-electric transducer (Karl Stetson Associates) is voltage driven by a National Instruments PCI-6024E DAQ board in the computer. The 640x480 pixel CCD camera (COHU) is connected to a National Instruments PCI-1408 IMAQ (frame-grabber) board in the computer. The strain gage signal-conditioning box (National Instrument SC-2043-SG) containing the excitation circuit and Wheatstone bridge is connected to the PC as well, and strain data are read synchronized with the acquisition of the frame grabber. DSPI system calibration was performed using a plate that is rotated by a lever and a micrometer having a sensitivity of 0.0001" [13].

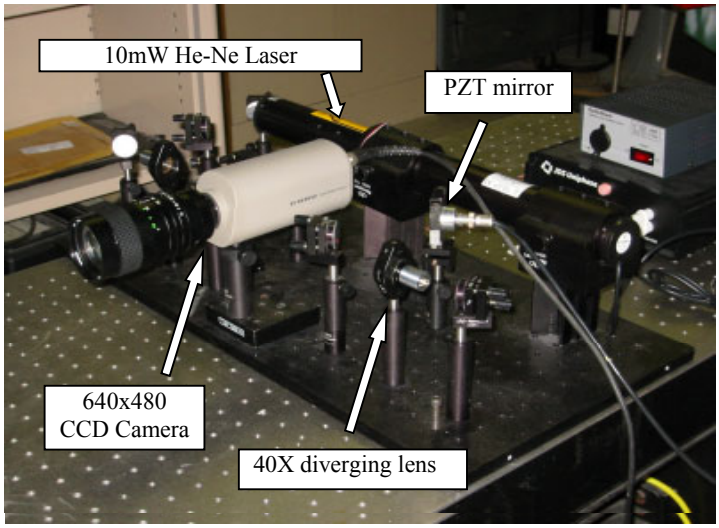

Figure 5. DSPI Setup used for the investigation. The schematic diagram is in Figure 1

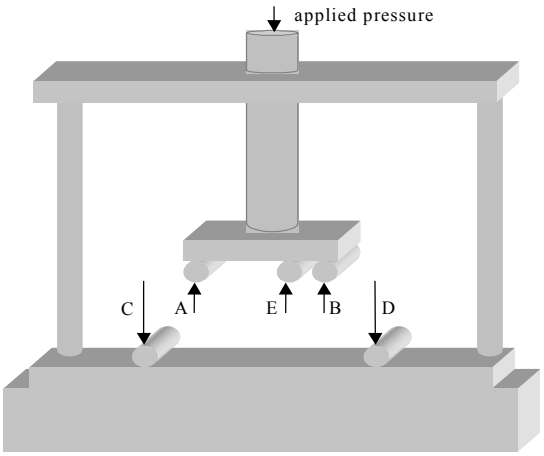

Figure 6. Loading apparatus schematic. (A,B,C,D correspond to 4-point bending and E,C,D to 3-point, as in Figure 4)

With the DSPI calibrated, experimentation began. First the surface specimen was tested. Two half-bridges were setup consisting of the two strain gages on the loaded surface specimen and two more on the "dummy" embedded specimen for temperature compensation. Several phase difference maps were acquired at various strain gage readings to observe possible variations in the readings. A non-speckled picture was also acquired in order to lay out a grid to use for unwrapping. The method was verified by comparing the DSPI results to the RSG results.

The embedded specimen was then ready to be tested using the surface specimen as the dummy instead. The embedded specimen was placed in the loading apparatus so that the object plane was at the shallowest depth within the specimen (thin-side). Several phase difference maps were acquired at various RSG strain readings. A non-speckled picture was also acquired for grid layout. The DSPI and RSG data were then compared. The specimen was then flipped around about the *y*-axis and reloaded. This time however, the object plane was at the deepest depth within the specimen (thick-side). Data acquisition procedures mirrored those used in obtaining thin-side data.

RESULTS

The data presented here will be limited to include only one sample from each test, as most results are similar. Each sample here was taken from a different "data set". Data sets differ by factors such as the day testing was performed, the type of loading used and specific loading conditions, and variations in transient effects. Each sample presented here is an accurate representation of the general trends within each data set.

First, the surface specimen results are presented. Following that, data related to both the thin-side and thick-side planes, corresponding to the embedded specimen, are presented. Table 1 displays the strain gage readings for all cases presented here; all data are from four-point bending tests.

RSG readings. ($\mu\varepsilon$)			
Strain Gage	Surface	Thin	Thick
Top (Compression)	-70	-97	-80
Bottom (Tension)	74	98	85

Table 1. Strain gage readings for the cases presented below.

Under pure bending theory, we expect to see a strain distribution varying linearly from minimum strain at the compression edge to maximum at the tension edge; this is what is assumed for the RSG readings by a linear trendline. The top is, of course, in compression and the bottom in tension. *Figure 7* displays the filtered phase difference map of the surface data given and *Figure 8* presents the RSG and DSPI strain results for the surface data. Further, *Figure 9* presents the RSG and DSPI strain results for the thin-side data, and *Figure 10* presents the RSG and DSPI strain results for the thick-side data. In each graph, a linear trendline has been applied to the DSPI and RSG data for comparison purposes along with an extrapolated DSPI reading at the strain gage and %-differences between the RSG and DSPI data at the gages.

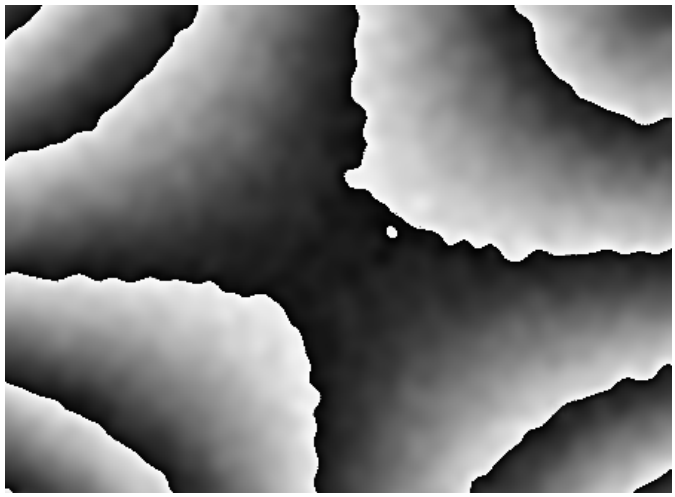

Figure 7. Sample filtered phase difference map. Corresponds to the data in Figure 8.

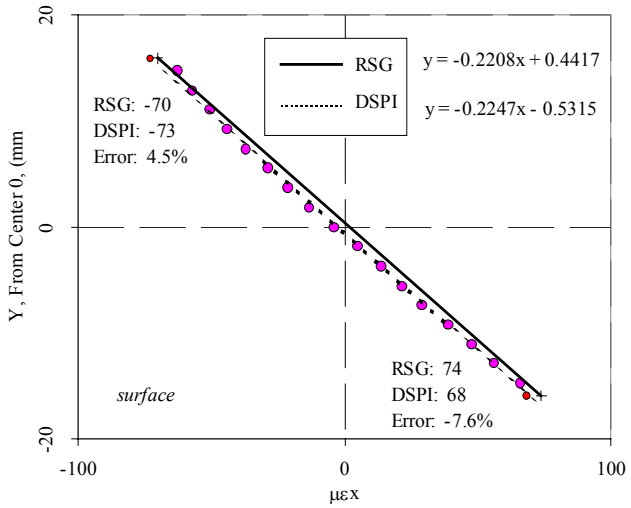

Figure 8. Sample RSG (+) and DSPI (o) data for the surface specimen.

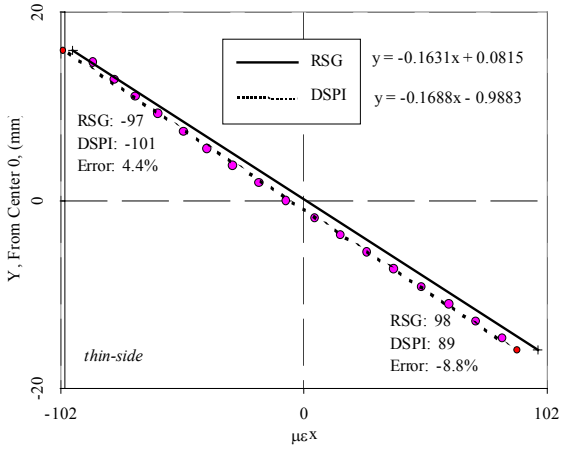

Figure 9. Sample RSG (+) and DSPI (o) data for the thin-side of the embedded specimen.

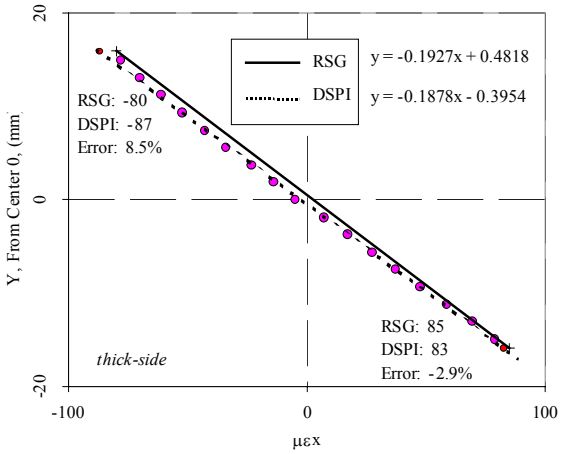

Figure 10. Sample RSG (+) and DSPI (o) data for the thick-side of the embedded specimen.

DISCUSSION

The underlying factors in this work that may have an effect on the outcome are the set-specific loading conditions, the material properties, and the interferometer setup. First and most likely, the largest factor is that of the loading. There were several inconsistencies including a minute asymmetry of the specimen, the difficulties arising due to the loading frame being composed of two separate pieces not including the specimen itself, and the fact that the specimen was placed in and situated within the frame by hand and eye. These issues are perhaps the most vital in this work with respect to results. Basically, set to set, the loading conditions changed slightly, therefore, due to the high sensitivity of DSPI, these slight variations led to sometimes-critical variations in the DSPI results obtained.

Moving on to the factor of the material properties, many issues arise. These issues include birefringence, both natural and stress induced, diffraction, and mechanical properties such as Poisson's ratio. Of course none of these issues may be changed within a material, though there are some corrections that can be made or the situation idealized by choosing a material with properties optimal to the design. Here acrylic has been chosen because of its optical clarity and its low birefringence, and no apparent optical effects have arisen in these pilot tests.

The interferometer setup creates a few compounding errors. Spherical non-collimated wavefronts were used; this creates both *z-* and *y-* displacement sensitivity as well as possible distortions caused by a varying sensitivity vector and errors induced by a change in the incidence angle. The errors caused by these issues may be decreased by using collimating lenses in the beam paths. Even further, aberrations in the zoom lens may cause field curvature of the interferometric data; however, tests have been performed and no apparent field distortions are present.

Two comparisons are made here; first the comparison between RSG and DSPI readings within each test, and second, the comparison of trends between each test. As can be seen by examination of *Figure 8* through *Figure 10*, all data are in excellent agreement.

When considering the comparison of RSG to DSPI data within each test, let us first take into consideration the difference between RSG and DSPI data at the gage; these differences range from ~3% to ~9%. The assumption made is that the interpolated DSPI readings at the gages are obtained using a linear trendline fitted to the data, corresponding again to beam theory. Clearly though, by examination of each plot, there can be seen a slight bowing in the DSPI data. It could therefore be said that if this bowing trend were continued, then the data could perhaps be more accurate, though the opposite could be true as well. However, regardless of this trend issue, the errors are very low and the data within each plot are fairly smooth and lack scattering.

Comparing between sets, it is seen that the agreement between the general data trends is excellent. All three plots exhibit the same general DSPI bowing, both in the same direction and on the same side of the RSG trendline. Further, set-to-set, the %-differences are very similar except for the errors of the thick side, which are roughly transposed in magnitude. This difference however is no issue and most likely due to slightly different specific loading conditions.

CONCLUSIONS

A new method of Digital Speckle Pattern Interferometry (DSPI) has been developed to measure an interior displacement field of an optically clear material in three- and four- point bending. This technique is termed *Embedded DSPI*. Specifically, an in-

plane-sensitive phase-stepped digital speckle pattern interferometer is used along with a PMMA specimen that contains an internal reflecting-scattering surface. The idea is to illuminate the scattering surface through the material and obtain a valid interference map. Once the phase difference map is obtained, the displacement is known, and this is then used to determine the strain. Electrical resistance strain gages (RSGs) are used here to verify the DSPI data.

The interferometer is sensitive to displacement in the *x*-direction. A four-step phase shifting algorithm has been used to calculate the phase difference maps. The phase difference maps are locally unwrapped and mean filtered to obtain clean wrapped phase difference maps with sharp 2π fringe edges. These maps are used to determine the strain along the y-axis using a method of line-unwrapping and least-square polynomial fitting and differentiation. DSPI data are plotted and compared versus RSG data and other DSPI data.

The technique is performed on a "surface" specimen and on an "embedded" specimen. The embedded specimen contains the scattering surface in its interior with one side of the specimen thicker than the other. The surface data are used as a reference as no optical effects would occur at the surface. The thought is that if the material exhibits any optical effects on wavefront propagation and beam interference, then a variation would show up between thick and thin material thicknesses.

Upon inspection of the experimental data obtained, it is concluded first that Embedded DSPI does yield valid interior displacement field data. The following observations are used to support this conclusion: that an apparently valid phase difference map is obtained for each test, and, the DSPI data obtained is in good agreement with RSG data in most cases, with errors averaging only ~9%. The second conclusion made is that the technique of Embedded DSPI is, in-fact, a reliable option for three-dimensional strain analysis. The following are used to justify this conclusion. Foremost, all data sets contain very consistent data within each respective set. Also, if loading conditions are taken into consideration, the trend differences between data sets can explained away; so that, if precision setups are used from set to set, one should obtain even more consistent results from set to set. And, lastly, there are no apparent material optical effects on the data stemming from the comparison of surface to thin to thick data.

Compared to other available techniques, such as three-dimensional photoelasticity or embedded-grid moire', the proposed embedded DSPI is fast to set-up and easy perform.

In conclusion, DSPI is a most valuable tool for the analysis of strain fields and this work using Embedded DSPI implies a promising future for this technique in the analysis of internal strain fields.

REFERENCES

[1] J.W. Dally, W.F. Riley, *Experimental Stress Analysis*, McGraw-Hill, 1991

[2] J.W. Dally, W.F. Riley, "Initial studies in three-dimensional dynamic photoelasticity", *Journal of Applied Mechanics*, Vol. 34, 2: 405-410 (1967)

[3] J.C. Dupré, and A. Lagarde, "Photoelastic Analysis of a Three-Dimensional Specimen by Optical Slicing and Digital Image Processing", *Experimental Mechanics*, Vol. 37, 4: 393-397 (1997)

[4] A.J. Durelli, and I.M. Daniel, "A nondestructive Three-Dimensional Strain Analysis Method", *Journal of. Applied Mechanics*, Vol. 23, 3: 83-86 (1961)

[5] R.C. Kerber, and J.S. Whittier, "Moiré Interferometry with Embedded Grids-Effect of Optical Refraction", *Experimental Mechanics*, Vol. 9, 5: 203-209 (1969)

[6] C. Bremond, and A.J. Durelli, "Experimental Analysis of Displacements and Shears at Surfaces of Contact", *Experimental Mechanics*, Vol. 21, 3: 105-110 (1981)

[7] C.A. Sciammarella, and F.P. Chaing, "The Moiré Method Applied to Three-Dimensional Elastic Problem", *Experimental Mechanics*, Vol. 4, 11: 313-319 (1964)

[8] G.L. Cloud, S. Paleebut, "Surface and Internal Strain Fields Near Coldworked Holes Obtained by a Multiple Embedded-Grid Moiré Method", *Engineering Fracture Mechanics*, Vol. 19, 2: 375-381 (1984)

[9] Cloud, G. and Paleebut, S., "Surface and Interior Strain Fields Measured by Multiple-embedded-grid Moiré and Strain Gages," *Experimental Mechanics*, Vol. 32, 3: 273-281 (1992)

[10] G.L. Cloud, *Optical Methods of Engineering Analysis*, Cambridge University Press, 1998

[11] S.S. Hong, F. Lanza di Scalea, G.L. Cloud, "Image processing algorithms for whole field strain measurement by ESPI", *Proc. Society for Experimental Mechanics 1998 Spring Conference*, Houston, Texas 1998

[12] H.A. Vrooman, and A.M.Maas, "Image processing algorithms for the analysis of phase-shifted speckle interference patterns", *Applied Optics*, Vol. 30, 13: 1636-1641 (1991)

[13] G.L. Cloud, "Practical Speckle Interferometry for measuring in-plane deformations", *Applied Optics*, Vol. 14, 4: 878-884 (1975)